Key words: Vehicle dynamics, interconnected suspension, multibody dynamics

BRUCE P. MINAKER [1] *, ZHENG YAO* [1]

DESIGN AND ANALYSIS OF AN INTERCONNECTED SUSPENSION FOR A SMALL OFF-ROAD VEHICLE

The paper describes the design and multibody dynamic analysis of a mechanically interconnected suspension, as applied to a small off-road vehicle. Interconnected suspensions use some sort of connection between the axles of a vehicle in order improve ride quality or vehicle handling. In principle, the connection may be hydraulic, pneumatic, or mechanical, but for installation in a typical passenger car, a mechanical connection would likely be impractical due to weight and complexity. In this paper, the vehicle in question is the University of Windsor SAE Baja off-road competition vehicle, and novel mechanical design is proposed. A multibody dynamic analysis is performed on the proposed design using the EoM open source multibody software developed by the University of Windsor Vehicle Dynamics and Control research group in order to assess any potential performance improvements.

1. Introduction

The conventional vehicle suspension system in use today has one flexible connection between each wheel and the vehicle chassis, typically a mechanical coil spring with a hydraulic damper in parallel. In addition, many vehicles will add an additional flexible coupling, called a sway bar, or more precisely, an anti-roll bar, between the left and right hand sides of the front axle, or the rear axle, or sometimes both axles. This is typically done using a torsional spring, and serves two purposes. First, if the main springs of the vehicle are chosen sufficiently soft enough to allow good ride quality, they will often not be firm enough to control body roll during cornering. Excessive body roll can have adverse affects on tire grip, and can contribute to increased load transfer, or, in an extreme scenario, rollover. It is

[1] *Department of Mechanical, Automotive & Materials Engineering, University of Windsor, Windsor ON N9B 3P4, Canada. Emails: bminaker@uwindsor.ca, yao113@uwindsor.ca*

best avoided if possible. Secondly, the ratio of the front to rear roll stiffness can be modified using the anti-roll bar. It is important to note that the anti-roll bar stiffness has a small effect on total lateral weight transfer, but a significant effect on the roll stiffness ratio of the front and rear axles. The roll stiffness ratio will influence the handling properties of the vehicle, with a high front roll stiffness contributing to an understeering and stable response; conversely, a high rear roll stiffness will contribute to an oversteering and very responsive, but potentially unstable, vehicle behaviour. For this reason, most passenger vehicles will use a front axle mounted anti-roll bar.

When selecting the spring stiffnesses during a vehicle design, it is quite common to use a 'bounce-pitch-roll' model, where the vehicle is treated as a single rigid body with three degrees of freedom, and each wheel is permitted an additional vertical motion, giving a seven degrees-of-freedom model. When a modal analysis on this type of model is performed, a there are a number of interesting results. Typically, the modes will be divided into two groups based on their frequency. Three low frequency motions, typically 0.5~2 Hz, are expected, where the response is largely chassis motion in the three bounce, pitch, and roll directions. Additionally, there are four high frequency motions, usually 8~12 Hz, that consist of mostly of wheel motion, referred to as 'wheel-hop'. The high frequency modes do not usually align to each wheel, but rather form a set of four coupled motions. These are: 1) bounce, all wheels moving in phase, 2) pitch, front and rear out-of-phase, 3) roll, left and right out-of-phase, and 4) twist or warp, diagonally opposite pairs out of phase.

The desired characteristics of the three primary chassis motions will generally dictate the bounce, pitch, and roll stiffnesses, e.g., high roll stiffness is desired for the resistance to lateral loads during cornering, low bounce stiffness provides good ride quality, etc. The warp stiffness is often ignored, as conventional suspension design does not allow for individual selection of the stiffness in each of these wheel hop modes. However, there is no need for a high warp stiffness, as it is only encountered when the road or track is uneven. In fact, by reducing the warp stiffness, it is possible to reduce the stiffness of a single wheel deflection, and the overall response of the suspension to rough terrain can be improved. However, in order to decouple these motions, an interconnected suspension is required.

A number of researchers have discussed the concept of decoupling the bounce, roll, pitch, and twist stiffnesses by using interconnected suspensions. Papers by Zapletal [1] in 2000, and Buj [2] in 2002 lay out many of the basic ideas, and describe the advantages of interconnected suspensions, particularly for racing applications. Zapletal was awarded a patent on a 'Balanced Suspension System' in 2004.

Nevertheless, there are very few instances of production passenger vehicles using interconnected suspensions, other than the typical anti-roll bar. They include the Citroën 2CV, which employed a mechanical interconnection of the main suspension coil springs on each side of the vehicle. The springs were arranged such

that they lay in the floor of the vehicle and were oriented longitudinally. British Leyland marketed vehicles using the Moulton Hydragas interconnected suspension, which functioned similarly to the Citroën system, and was primarily intended for improvement of ride quality by coupling front and rear suspensions, particularly for vehicles with short wheelbases. Typically, passengers find pitch motions to be more uncomfortable than bounce motions, which partially explains why a longer wheelbase vehicle tends to have a better ride quality. Linking the front and rear suspensions so that they tend to move in opposing directions generates a similar effect. When the front suspension moves up to absorb a bump, the compression of the front spring pushes the front of the chassis up. The interconnection simultaneously pushes down on the rear suspension, and in reaction, lifts the rear of the vehicle in concert with the front. In 2003, Rideout and Anderson published a model of the Moulton Hydragas interconnected suspension [3].

Kinetic Pty Ltd and Tenneco Automotive implemented a hydraulic interconnected suspension that was utilized by both Citroen in the World Rally Car series, and by Mitsubishi in the Dakar Rally event. This implementation provided such an advantage that in 2006, the organizers of both events banned interconnected suspensions. The Lexus GX470 and Toyota Land Cruiser featured similar systems, under the trademark Kinetic Dynamic Suspension System. In 2005 and 2006, Wilde et. al. published studies on the performance of the Kinetic™ system [4, 5], particularly as a means for avoiding rollover in sport utility vehicles.

A number of other researchers have continued to explore the benefits of coupled suspensions, with the primary focus on the hydraulic style of implementation, e.g., Smith and Walker [6], Mavroudakis and Eberhard [7], and Cao et. al. [8].

2. SAE Baja

The SAE Baja is an annual design challenge event hosted by SAE International, as a part of their Collegiate Design Series, where teams of undergraduate and graduate engineering students design, analyze, build, test and compete in small off-road style race cars. It is very popular amongst Canadian and U.S. based engineering schools, with around 100 teams competing. The University of Windsor has been fielding an entry continuously since 2000. One of the challenges in the SAE Baja event is the design of a suspension system suitable for performance and driver comfort over very rough terrain. For several years, the University of Windsor SAE Baja car has used a double A-arm style front suspension, and independent trailing arm rear suspension. This paper discusses a proposal for a novel Baja vehicle design incorporating an interconnected suspension. The vehicle design is developed using the 3D CAD software CATIA, and analyzed using the Equations of Motion (EoM) multibody dynamics software, to evaluate the effect of the interconnection.

The design is based on a coupling of the anti-roll bar between the front and rear suspensions. Typically, the anti-roll bar will be mounted to the chassis using

two bushings, and the two ends of the bar will be attached to the left and right side suspension arms. Deflection of the suspensions in opposing directions results in a twist of the anti-roll bar, and a corresponding resistance force. Deflection of the suspensions in the same direction simply rotates the bar freely in its mounting bushings, so as not to contribute to bounce stiffness.

In this new proposed variation of the design, the anti-roll bar is not mounted directly to the chassis, but rather to a pair of bell-cranks that are in turn mounted to the chassis. The anti-roll bar sits in a location very near to that of a conventional front mounted bar. The bell-cranks that carry the anti-roll bar are driven by deflection of the rear suspension. As a result, if the suspension motion is such that that axles are rolling in the same direction, as they would during a cornering manoeuvre, then the mounts move so that twist of the anti-roll bar is increased. If the suspension motion is such that the axles are rolling in opposing directions, as they would when a single wheel strikes a bump, the mounts move so that the twist of the anti-roll bar is reduced. An image of the CATIA model is shown in Fig. 1 and annotated in Table 1.
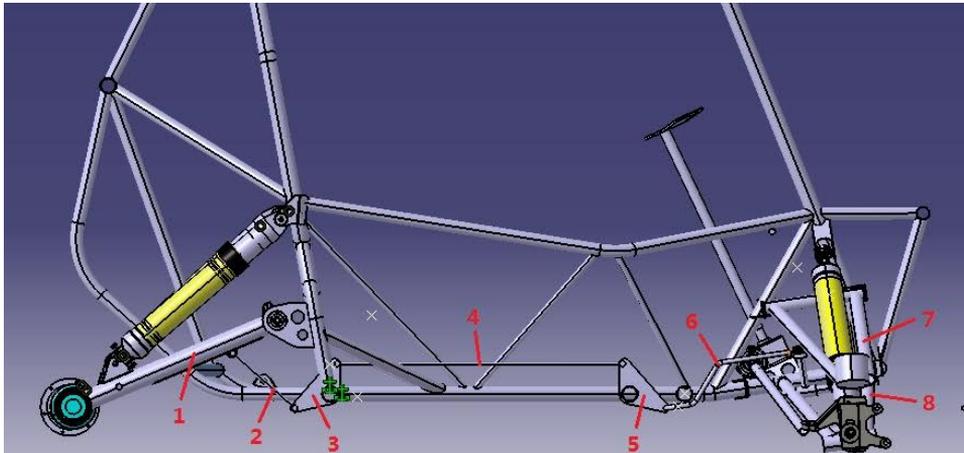

Fig. 1. CATIA model of Baja car showing interconnection

Table 1.
Annotation

No.	Body name
1	Trailing arm
2,4	Connecting link
3,5	Bell-cranks
6	Anti-roll bar
7	Upper A-arm
8	Lower A-arm

3. Dynamic Model

The dynamic model of the vehicle is an extension of the one described in [9]. It has 13 degrees of freedom, and is composed of 20 rigid bodies. The degrees of freedom are all six motions of the chassis, plus four suspension motions, and two front wheel rotations. The rear wheels can also rotate, but are driven by a common axle. The model may be more precisely described as 12.5 degrees of freedom, as forward speed is held constant by a nonholonomic constraint.

The bodies modelled are the chassis, each of the four wheels, an upper and lower A-arm and upright for each front suspension, a trailing arm for each rear suspension, and a drive axle coupling the rear wheels together. There are four bell-cranks that are added to drive the motion of the anti-roll bar, and two bodies that are used to represent the mass of the anti-roll bar. The body information is given in Tables 2 and 3. The mass and moments of inertia properties are produced from the CATIA solid model, based on the size and materials of the components.

Table 2.

Body locations

No.	Body name	Location [m]		
1	Chassis	0.260,	0.000,	0.568
2	Upper A-arm	0.994,	0.318,	0.435
3	Lower A-arm	1.041,	0.378,	0.268
4	Upright	1.039,	0.578,	0.279
5	Front wheel	1.041,	0.658,	0.253
6	Trailing arm	−0.321,	0.434,	0.291
7	Rear wheel	−0.524,	0.600,	0.253
8	Front bellcrank	0.651,	0.255,	0.279
9	Anti-roll bar	0.700,	0.255,	0.240
10	Rear bellcrank	0.028,	0.360,	0.279
11	Axle	−0.524,	0.000,	0.253

Note: values are given for the left hand side of the vehicle only, as the vehicle is treated as symmetric

The total number of holonomic constraints in this model is 107, applied through 22 connections. The baseline vehicle has 71 constraints, while the interconnection system has 36. Each of the upper and lower A-arms is connected to the vehicle body using a revolute joint; they can rotate around the longitudinal axis. Two ball joints on each side connect the upper and lower A-arms to the upright. Each front wheel is attached to its upright through a revolute joint around the lateral axis. Finally, a tie rod (modelled as a massless rigid link) connects each upright to the vehicle body. For the rear suspension, one revolute joint connects each swing arm to the chassis, allowing only rotation around the lateral axis. Similarly to the front wheels, each rear wheel is attached to a swing arm and can also only rotate around the lateral

Table 3.

Body properties

No.	Body name	Mass [kg]	Inertia [kg·m^2]		
1	Chassis	200.000	27.000,	61.000,	61.000
2	Upper A-arm	0.683	0.008,	0.005,	0.010
3	Lower A-arm	1.538	0.036,	0.014,	0.039
4	Upright	0.640	0.001,	0.001,	0.001
5	Front wheel	5.556	0.134,	0.236,	0.134
6	Trailing arm	3.133	0.020,	0.112,	0.104
7	Rear wheel	5.556	0.134,	0.236,	0.134
8	Front bellcrank	0.090	0.000,	0.000,	0.000
9	Anti-roll bar	0.090	0.000,	0.000,	0.000
10	Rear bellcrank	0.090	0.000,	0.000,	0.000
11	Axle	5.000	0.338,	0.010,	0.338

Note: inertia values are I_{xx}, I_{yy}, I_{zz}, all cross-products of inertia are neglected

axis. The drive axle is attached to the rear wheels using a constant velocity (CV) joint at each end, with one end also restricting lateral motion of the axle. Finally, a single nonholonomic constraint is added to enforce a constant forward speed at the centre of mass of the chassis.

The mechanical interconnection starts by mounting each of four bell-cranks to the chassis with a revolute joint. Each of the rear bell cranks is connected to a rear trailing arm by a push-rod modelled as a massless rigid link, and to the front bell-crank on the same side, by another massless rigid link. Each of the front bell-cranks carries a small body representing the mass of the anti-roll bar; these small bodies are constrained to their respective bell-cranks by a revolute joint. Each of the anti-roll bar bodies is then driven by a short massless rigid link connected to a front lower control arm, representing the physical drop-link. The number of constraints in each connection is detailed in Table 4.

The two bodies that represent the anti-roll bar are connected with a torsional spring running laterally across the chassis with a stiffness of 2000 Nm/rad. The front and rear shock absorbers are all modelled as springs with stiffness, damping, and non-zero free length. The spring stiffness is set 20 000 N/m, with a damping value of 1000 Ns/m, at both the front and the rear. Each tire is modelled as a bushing, which works like a spring with no free length. The tire has stiffness in the vertical direction, and damping in both horizontal directions, to represent a linear force vs. slip tire model. The vertical stiffness is 75 000 N/m and the horizontal damping is 5000 Ns/m at all four tires (equivalent to a tire cornering stiffness of 25 000 N/rad and a longitudinal slip stiffness of 25 000 N at 5 m/s).

The weight of all the bodies is used to compute the preload in all connectors, and the associated tangent stiffness matrix. The tire-road contact is defined as the periphery of a disk, in the plane of the wheel. The effect of the contact geometry,

Table 4.

Connection locations

No.	Connection name	Location [m]			Constraints
1	CV joint	−0.524,	0.450,	0.253	4
2	Upper A-arm hinge	0.976,	0.212,	0.476	5
3	Lower A-arm hinge	1.018,	0.185,	0.309	5
4	Upper ball-joint	1.040,	0.539,	0.350	3
5	Lower ball-joint	1.060,	0.568,	0.207	3
6	Front wheel bearing	1.041,	0.686,	0.253	5
7	Trailing arm bearing	−0.092,	0.429,	0.368	5
8	Rear wheel bearing	−0.524,	0.492,	0.253	5
9	Front bellcrank mount	0.651,	0.255,	0.279	5
10	Rear bellcrank mount	0.028,	0.360,	0.279	5
11	Anti-roll bar mount	0.700,	0.255,	0.240	5
12	Front tire	1.041,	0.658,	0.000	0
13	Rear tire	−0.524,	0.600,	0.000	0
14	Constant speed	0.260,	0.000,	0.568	0.5
15	Rear shock	−0.087,	0.445,	0.672	0
–	Rear shock	−0.507,	0.445,	0.316	–
16	Front shock	0.947,	0.252,	0.652	0
–	Front shock	1.048,	0.467,	0.243	–
17	Anti-roll spring	0.700,	0.255,	0.240	0
–	Anti-roll spring	0.700,	−0.255,	0.240	–
18	Tie-rod	0.840,	0.206,	0.376	1
–	Tie-rod	0.960,	0.564,	0.274	–
19	Rear link	−0.021,	0.360,	0.240	1
–	Rear link	−0.140,	0.434,	0.310	–
20	Side link	0.651,	0.255,	0.328	1
–	Side link	0.028,	0.360,	0.328	–
21	Front drop link	0.970,	0.270,	0.304	1
–	Front drop link	0.970,	0.270,	0.240	–

Note: coordinate values are given for the left hand side of the vehicle only, right side constraints are symmetric in all cases except the axle CV joint, which has one additional constraint on the left side

although, is simple, is important, as it also factors into the tangent stiffness matrix. As a result, the natural tendency of the tire to 'fall over' side-to-side, and not front-to-back, is captured. The equations are generated around a constant forward speed of 5 m/s, with the associated angular velocity of the wheels and axle, to capture the gyroscopic effects.

A total of five virtual sensors are included in the vehicle model. Three sensors are fitted at the right front wheel, to measure the absolute vertical motion of the chassis, the relative vertical motion between the chassis and the wheel, and the

relative vertical motion between the wheel and the ground, i.e., the tire compression. The remaining two sensors are the right rear tire compression and the roll angle of the chassis. The motion is driven by two actuators. The first actuator is placed between the front tire and the road, to simulate road disturbances, and the second is a pure rolling moment acting directly on the chassis. In order to allow a direct comparison of inputs and outputs in a frequency response style analysis, the roll angle output (in radians) is scaled by the track width of the vehicle to produce a measure of roll in units of linear displacement (the relative vertical displacement of the ground across the vehicle that would give the same roll angle, if the vehicle were at rest). Similarly, the input moment is generated by a signal that was scaled by the track width and the tire vertical stiffness, such that the input signal also has units of linear displacement.

3.1. Vehicle Configurations

In order to assess the contribution of the coupled suspension system, the vehicle is analyzed in three configurations. First, the analysis is done with no interconnection, and simply the four main suspension springs in place. In the second configuration, the interconnection system is added, with the intent of significantly increasing the roll stiffness without a corresponding increase in twist stiffness, and having a minimal effect on roll stiffness distribution. Finally, a third configuration with a traditional front mounted anti-roll bar is added. In the third configuration, the torsional stiffness of the anti-roll bar is 4000 Nm/rad, twice that in the second configuration, in order to maintain a comparable increase in roll stiffness.

4. Formulation of the Equations of Motion

The equations of motion of the vehicle are formed using the EoM software. The EoM code, described in [9], is developed by the University of Windsor Vehicle Dynamics and Control Research Group, and has successfully solved a number of benchmark problems. It is capable of analyzing three dimensional multibody mechanical systems with many degrees of freedom, to generate linear or linearized equations of motion.

The software is entirely open source and runs within MATLAB® or Octave. The input of the software is a simple function file describing the system in question, in terms of the inertial, geometric, stiffness and damping properties. The output is the state space form of the equations of motion, and optionally, a report tabulating the results of a linear analysis in a .pdf format, and animations of the mode shapes that can be viewed using any virtual reality modelling language (VRML) viewer.

When analyzing a multibody system, EoM will first read the information from the input data, and build the necessary stiffness and constraint Jacobian matrices required to find all the preload and constraint forces. Once these are known, the stiffness matrices are updated with the tangent stiffness terms. The kinematic

differential equations relating position and velocity are then combined with the Newton-Euler equations of motion, reduced to a minimal coordinate set, and cast in the following form:

$$\begin{bmatrix} \mathbf{E} & \mathbf{0} \\ \mathbf{0} & \mathbf{I} \end{bmatrix} \begin{Bmatrix} \dot{x} \\ y \end{Bmatrix} = \begin{bmatrix} \mathbf{A} & \mathbf{B} \\ \mathbf{C} & \mathbf{D} \end{bmatrix} \begin{Bmatrix} x \\ u \end{Bmatrix} \tag{1}$$

A careful examination will show that this system, known as the descriptor form of the state space, can be easily reduced to the standard state space form, if the $\mathbf{E}$ matrix is non-singular. In the event of singularities, then the system becomes a set of differential-algebraic equations. Nevertheless, a singular value decomposition approach can be used to reduce the system to an equivalent lower dimensional standard state space form. From this state matrix form, EoM will perform a number of linear analyses, e.g., calculate the eigenvalue of each mode to determine the stability.

5. System Response

Three analyses are conducted on the resulting system of equations: a modal analysis, a frequency response analysis, and a steady state analysis.

5.1. Modal Analysis

The first step in the analysis determines the natural frequencies, damping ratios, and time constants of the motions. A simple accounting of the modes is conducted first. Six motions per body, for 20 bodies, gives 120 equations of motion. The holonomic constraints remove 107, leaving 13 degrees of freedom. Each degree of freedom is modelled with a second order equation; this implies 26 eigenvalues, less one from the nonholonomic constraint, giving 25 in total. Of these 25, 14 appear as complex conjugate pairs, representing seven oscillatory modes. The remaining 11 appear as five negative real roots, or non-oscillatory overdamped motions, and six zero roots or rigid body modes. The results show that three of the oscillatory modes are the expected low frequency chassis motions of bounce, pitch and roll, along with four high frequency wheel hop motions. The five damped motions consist of combinations of yaw velocity, lateral velocity, and wheel angular velocities. The six rigid body modes are similar, combining yaw displacement, lateral displacement, longitudinal displacement, and wheel angular displacements. Note that longitudinal velocity does not appear in the modes, as it is removed by the nonholonomic constraint.

For the baseline configuration, the frequencies are 1.87 Hz for bounce, 2.64 Hz for pitch, and 1.78 Hz for roll. The results for the configurations with modification are almost identical. The bounce and pitch frequencies are unchanged, as are the wheel hop frequencies for those modes that contain bounce and pitch motions. This

is expected as the suspension couplings have no effect on bounce or pitch stiffness. The roll frequencies increase to 2.13 Hz and 2.08 Hz for the interconnected and anti-roll bar configurations respectively. The increase in roll frequency shows both methods effectively increase roll stiffness. In all cases, the frequencies are in a reasonable range, although somewhat high, due to the light weight of the Baja vehicle in comparison to a normal passenger car.

The roll and twist wheel hop frequencies remain relatively constant in the three configurations, as they are primarily determined by the tire stiffness, which is much larger than the suspension stiffness, and masks the effects of changes in suspension parameters. As the warp motion of the suspension appears only in the wheel hop modes, the distinction between the two configurations with modification

Table 5.

Eigenvalue analysis, baseline vehicle configuration

No.	Frequency [Hz]	Damping Ratio	Time Constant [s]
1	–	–	7.1029×10^{-4}
2	–	–	7.2508×10^{-4}
3	–	–	7.3252×10^{-4}
4	–	–	3.7579×10^{-3}
5	–	–	6.0248×10^{-3}
6	1.4204×10^{1}	1.6238×10^{-1}	6.9001×10^{-2}
7	1.4204×10^{1}	1.6238×10^{-1}	6.9001×10^{-2}
8	1.5563×10^{1}	3.2856×10^{-1}	3.1125×10^{-2}
9	1.5563×10^{1}	3.2856×10^{-1}	3.1125×10^{-2}
10	1.5490×10^{1}	2.4075×10^{-1}	4.2677×10^{-2}
11	1.5490×10^{1}	2.4075×10^{-1}	4.2677×10^{-2}
12	1.5909×10^{1}	2.3271×10^{-1}	4.2991×10^{-2}
13	1.5909×10^{1}	2.3271×10^{-1}	4.2991×10^{-2}
14	2.6421×10^{0}	2.7004×10^{-1}	2.2307×10^{-1}
15	2.6421×10^{0}	2.7004×10^{-1}	2.2307×10^{-1}
16	–	–	–
17	–	–	–
18	1.8705×10^{0}	2.9429×10^{-1}	2.8913×10^{-1}
19	1.8705×10^{0}	2.9429×10^{-1}	2.8913×10^{-1}
20	1.7798×10^{0}	3.2031×10^{-1}	2.7917×10^{-1}
21	1.7798×10^{0}	3.2031×10^{-1}	2.7917×10^{-1}
22	–	–	–
23	–	–	–
24	–	–	–
25	–	–	–

Note: a '–' character in all three columns indicates a rigid body mode, i.e., a zero eigenvalue, while in only the first two columns, it indicates an overdamped, nonoscillatory mode

Table 6.

Eigenvalue analysis, interconnected suspension

No.	Frequency [Hz]	Damping Ratio	Time Constant [s]
1	–	–	7.1029×10^{-4}
2	–	–	7.2508×10^{-4}
3	–	–	7.3252×10^{-4}
4	–	–	3.7673×10^{-3}
5	–	–	6.0253×10^{-3}
6	1.4204×10^{1}	1.6238×10^{-1}	6.9001×10^{-2}
7	1.4204×10^{1}	1.6238×10^{-1}	6.9001×10^{-2}
8	1.5606×10^{1}	3.2892×10^{-1}	3.1004×10^{-2}
9	1.5606×10^{1}	3.2892×10^{-1}	3.1004×10^{-2}
10	1.6292×10^{1}	2.2985×10^{-1}	4.2501×10^{-2}
11	1.6292×10^{1}	2.2985×10^{-1}	4.2501×10^{-2}
12	1.5490×10^{1}	2.4075×10^{-1}	4.2677×10^{-2}
13	1.5490×10^{1}	2.4075×10^{-1}	4.2677×10^{-2}
14	–	–	–
15	–	–	–
16	2.6421×10^{0}	2.7004×10^{-1}	2.2307×10^{-1}
17	2.6421×10^{0}	2.7004×10^{-1}	2.2307×10^{-1}
18	1.8705×10^{0}	2.9429×10^{-1}	2.8913×10^{-1}
19	1.8705×10^{0}	2.9429×10^{-1}	2.8913×10^{-1}
20	2.1279×10^{0}	2.6370×10^{-1}	2.8363×10^{-1}
21	2.1279×10^{0}	2.6370×10^{-1}	2.8363×10^{-1}
22	–	–	–
23	–	–	–
24	–	–	–
25	–	–	–

is not readily apparent in the natural frequency results. Tables 5–7 give the full eigenvalue results for the baseline, interconnected, and conventional front anti-roll bar configurations.

5.2. Frequency Response

Next, the models were analyzed using a frequency response approach. Results for the right front corner of the baseline model are shown in Fig. 2. The plot shows three frequency regions that can be loosely defined as: 1) low, below the body motion frequencies, 2) midrange, between the body motion and wheel hop frequencies, and 3), high, above the wheel hop frequencies. The plots show that at low frequencies, the irregularities in the road are mostly absorbed by motion of the chassis. Near the body motion frequencies, the chassis motion peaks, reaching val-

Table 7.

Eigenvalue analysis, anti-roll bar configuration

No.	Frequency [Hz]	Damping Ratio	Time Constant [s]
1	–	–	7.1029×10^{-4}
2	–	–	7.2508×10^{-4}
3	–	–	7.3251×10^{-4}
4	–	–	3.7641×10^{-3}
5	–	–	6.0246×10^{-3}
6	1.5566×10^{1}	3.2707×10^{-1}	3.1261×10^{-2}
7	1.5566×10^{1}	3.2707×10^{-1}	3.1261×10^{-2}
8	1.4207×10^{1}	1.6240×10^{-1}	6.8982×10^{-2}
9	1.4207×10^{1}	1.6240×10^{-1}	6.8982×10^{-2}
10	1.6545×10^{1}	2.2807×10^{-1}	4.2178×10^{-2}
11	1.6545×10^{1}	2.2807×10^{-1}	4.2178×10^{-2}
12	1.5490×10^{1}	2.4076×10^{-1}	4.2676×10^{-2}
13	1.5490×10^{1}	2.4076×10^{-1}	4.2676×10^{-2}
14	2.6417×10^{0}	2.6994×10^{-1}	2.2319×10^{-1}
15	2.6417×10^{0}	2.6994×10^{-1}	2.2319×10^{-1}
16	–	–	–
17	–	–	–
18	2.0752×10^{0}	2.7220×10^{-1}	2.8175×10^{-1}
19	2.0752×10^{0}	2.7220×10^{-1}	2.8175×10^{-1}
20	1.8707×10^{0}	2.9436×10^{-1}	2.8903×10^{-1}
21	1.8707×10^{0}	2.9436×10^{-1}	2.8903×10^{-1}
22	–	–	–
23	–	–	–
24	–	–	–
25	–	–	–

ues that are often larger than the size of the disturbance. In the midrange, the motion of the chassis starts decreasing, and the disturbance is now absorbed by relative motion of the suspension. Finally, at high frequencies, the chassis and suspension motion both decrease, and the disturbance is absorbed by tire deflection. Generally, the wider the midrange region, the better the vehicle suspension performs. Using chassis motion to absorb road irregularities leads to passenger discomfort, while using the tire can lead to loss of tire grip. However, care needs to be taken to avoid low frequencies that can cause passenger motion sickness.

Fig. 3 shows a comparison of the chassis motion for the three configurations in the low and midrange of frequencies. Note that the logarithmic nature of the plot may understate the differences in the responses. The plot shows that both the interconnected and anti-roll configurations perform worse than the baseline, especially in the 2~3 Hz band, but with some advantage to the interconnected
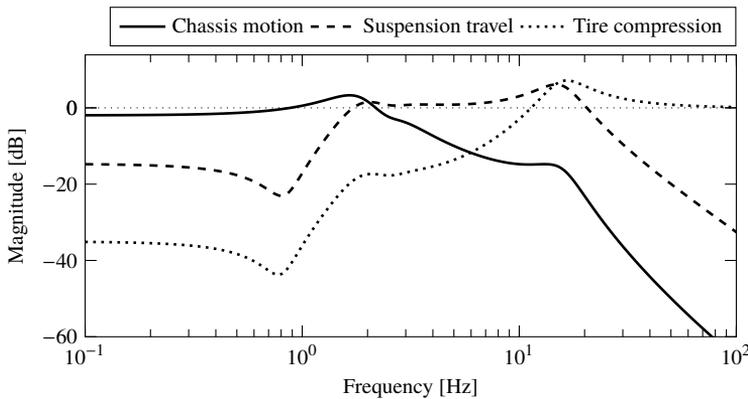
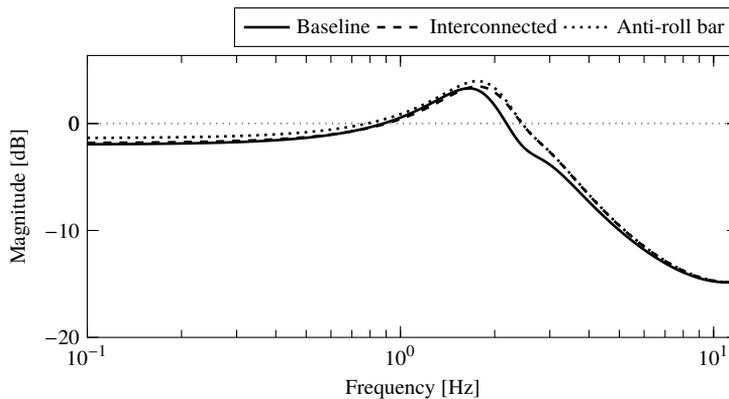Fig. 2. Frequency response of baseline vehicle at right front corner to road displacement

Fig. 3. Frequency response showing chassis motion of vehicle at right front corner in response to road displacement

arrangement. This is expected, as both the modified configurations have a higher roll stiffness than the baseline. The increase in roll stiffness typically comes with a ride performance penalty. Once the frequencies reach the midrange, the interconnected and anti-roll configurations are nearly identical.

Fig. 4 shows a comparison of the suspension motion for the three configurations, also in the low and midrange of frequencies. Again, the plot shows that both the interconnected and anti-roll configurations perform worse than the baseline, but with some advantage to the interconnected arrangement. Once the frequencies reach the midrange, all three configurations are nearly identical.

Fig. 5 shows a comparison of the tire compression for the three configurations, in the midrange and high frequencies. The plot shows that both the interconnected and anti-roll configurations perform worse than the baseline in the 2~3 Hz band, but little difference otherwise.
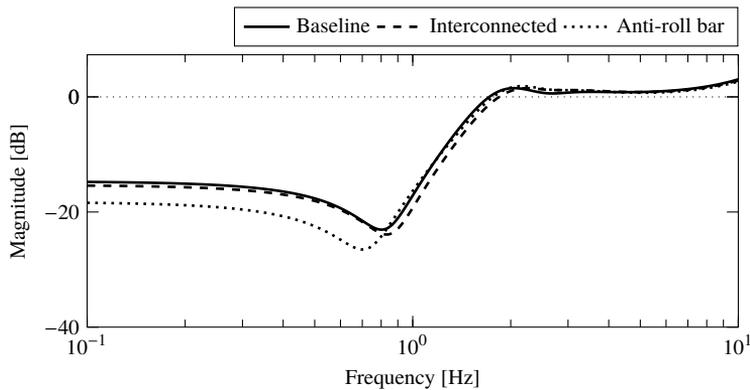
Fig. 4. Frequency response showing suspension displacement at right front corner in response to road displacement
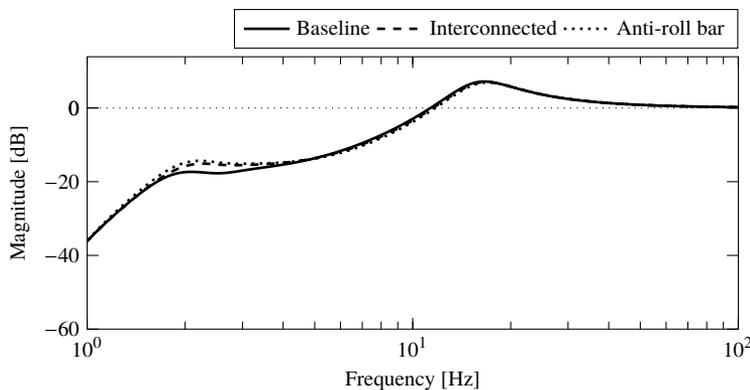

Fig. 5. Frequency response showing tire compression at right front corner in response to wheel bump

5.3. Steady State Transfer Functions

Finally, a steady state transfer function analysis was also completed. The results for the baseline vehicle configuration are shown in Table 8, the interconnected configuration is shown in Table 9, and the traditional anti-roll bar configuration is shown in Table 10.

The first noteworthy point is a comparison of the ratio of chassis roll angle to applied roll moment, i.e., the roll flexibility, which would be particularly relevant in a corners where rolling moments would be relatively sustained. The results agree with the eigenvalue analysis, showing increased roll stiffness in both the second and third configurations, with a ratio of 10.9 for the baseline, 7.66 for the inter-connected configuration, and 8.05 for the anti-roll bar configuration. Even with the

Table 8.

Steady state results for the baseline configuration

No.	Output/Input	Gain
1	Front chassis motion/Front wheel bump	7.9772×10^{-1}
2	Front chassis motion/Roll moment	5.4709×10^{0}
3	Front suspension travel/Front wheel bump	-1.8457×10^{-1}
4	Front suspension travel/Roll moment	4.9940×10^{0}
5	Front tire compression/Front wheel bump	-1.7714×10^{-2}
6	Front tire compression/Roll moment	4.7687×10^{-1}
7	Rear tire compression/Front wheel bump	-9.7282×10^{-1}
8	Rear tire compression/Roll moment	6.4054×10^{-1}
9	Roll sensor/Front wheel bump	-7.4539×10^{-1}
10	Roll sensor/Roll moment	1.0942×10^{1}

Note: the roll motion and moment are scaled by characteristic values such that they are expressed in units of length, and thus all the steady state values are unitless ratios

Table 9.

Steady state results for the interconnected configuration

No.	Output/Input	Gain
1	Front chassis motion/Front wheel bump	8.1043×10^{-1}
2	Front chassis motion/Roll moment	3.8304×10^{0}
3	Front suspension travel/Front wheel bump	-1.7141×10^{-1}
4	Front suspension travel/Roll moment	3.2971×10^{0}
5	Front tire compression/Front wheel bump	-1.8152×10^{-2}
6	Front tire compression/Roll moment	5.3334×10^{-1}
7	Rear tire compression/Front wheel bump	-9.7220×10^{-1}
8	Rear tire compression/Roll moment	5.6039×10^{-1}
9	Roll sensor/Front wheel bump	-7.1996×10^{-1}
10	Roll sensor/Roll moment	7.6609×10^{0}

increased torsional spring stiffness in the anti-roll configuration, the interconnected configuration is better at reducing roll in corners.

Another interesting result is the ratio of chassis motion to wheel input, as this is a direct measure of driver comfort. The results agree with the frequency response, showing in the steady state, the default configuration has the best road absorption with 79.8% of the road displacement at the chassis, while the interconnected and anti-roll bar configurations show 81.0% and 85.5% respectively. The interconnected suspension again incurs a small ride performance penalty to increase the roll stiffness, but less than the anti-roll bar configuration.

Finally, it is noteworthy to compare the ratio of front tire compression to rear tire compression in response to roll moment, as this is an indicator of the roll stiffness distribution. The tables show that the baseline is in the ratio of 0.477:0.641

Table 10.

Steady state results for front anti-roll bar configuration

No.	Output/Input	Gain
1	Front chassis motion/Front wheel bump	8.5456×10^{-1}
2	Front chassis motion/Roll moment	4.0235×10^{0}
3	Front suspension travel/Front wheel bump	-1.2209×10^{-1}
4	Front suspension travel/Roll moment	3.4031×10^{0}
5	Front tire compression/Front wheel bump	-2.3350×10^{-2}
6	Front tire compression/Roll moment	6.2042×10^{-1}
7	Rear tire compression/Front wheel bump	-9.6604×10^{-1}
8	Rear tire compression/Roll moment	4.6790×10^{-1}
9	Roll sensor/Front wheel bump	-6.3171×10^{-1}
10	Roll sensor/Roll moment	8.0470×10^{0}

or 43%:57%. The interconnected configuration has a ratio of 0.533:0.560 or 49%:51%. The anti-roll bar configuration has a ratio of 0.620:0.468 or 57%:43% ratio. Even though the roll stiffness is biased toward the rear in the baseline, it is close to balanced in the interconnected configuration, and front biased in the anti-roll bar configuration. These results confirm the expectations that added roll stiffness from the anti-roll bar on the front axle would shift stiffness bias toward the front, while the interconnected configuration distributes the roll stiffness more evenly, and does so with less effect on the twist stiffness.

6. Conclusions

Based on the results seen in the analysis, it appears that the interconnected suspension should offer a performance advantage compared to a conventional anti-roll bar configuration. However, this advantage disappears at high frequencies, implying that the system might be more suitable in off-road style applications, where the disturbances would tend to be of larger amplitude and lower frequency. The results confirm that such a system is capable of increasing roll stiffness independently from twist stiffness. The ride penalty from the increased roll stiffness is reduced in the interconnected configuration. Of course, the interconnected system adds some additional weight and complexity to the suspension, that should also be considered. If designed carefully, the weight penalty could be made relatively small, but the complexity would likely add to reliability concerns, especially in an off-road racing environment. The current analysis does not consider the stresses in the various components, which would be necessary before physical implementation. Additional non-linear time history simulations of the vehicle motion in various configurations conducted using a commercial software are planned for further investigation.

References

[1] E. Zapletal. Balanced suspension. *SAE Technical Paper* 2000-01-3572, 2000.

[2] J.F. Buj. Integral suspension system for motor vehicles based on passive components. *SAE Technical Paper* 2002-01-3105, 2002.

[3] G. Rideout, R.J. Anderson. Experimental testing and mathematical modeling of the interconnected hydragas suspension system. *SAE Technical Paper* 2003-01-0312, 2003.

[4] J.R. Wilde, G.J. Heydinger, D.A. Guenther, T.P. Mallin, A.M. Devenish. Experimental evaluation of fishhook maneuver performance of a kinetic suspension system. *SAE Technical Paper* 2005-01-0392, 2005.

[5] J.R. Wilde, G.J. Heydinger, D.A. Guenther. ADAMS simulation of ride and handling performance of the Kinetic™ suspension system. *SAE Technical Paper* 2006-01-1972, 2006.

[6] M.C. Smith, G.W. Walker. Interconnected vehicle suspension. *Journal of Automobile Engineering*, 219(3):295–307, 2005. doi: 10.1243/095440705X6578.

[7] B. Mavroudakis, P. Eberhard. Mode decoupling in vehicle suspensions applied to race cars. In *Proceedings of the III European Conference on Computational Mechanics Solids, Structures and Coupled Problems in Engineering*, Lisbon 2006.

[8] D. Cao, S. Rakheja, C.Y. Su. Roll and pitch-plane coupled hydro-pneumatic suspension. *Vehicle System Dynamics*, 48(3):361–386, 2010. doi: 10.1080/00423110902883251.

[9] B.P. Minaker, X. Yang, S. Li. Design optimization of an SAE Baja vehicle using the EoM open source multibody dynamics code. *Proceedings of The Canadian Society for Mechanical Engineering International Congress*, 2014.